Journal of Colloid and Interface Science 354 (2011) 359–363

Contents lists available at ScienceDirect

Journal of Colloid and Interface Science

www.elsevier.com/locate/jcis

Landau–Levich menisci

M. Maleki [a,b], M. Reyssat [b], F. Restagno [c], D. Quéré [b], C. Clanet [d,*]

[a] IASBS, P.O. Box 45195-1159, Zanjan 45195, Iran
[b] PMMH, UMR 7636 du CNRS, ESPCI, 75005 Paris, France
[c] LPS, UMR 8502 du CNRS, Université Paris Sud XI, 91400 Orsay, France
[d] LadHyX, UMR 7646 du CNRS, Ecole Polytechnique, 91128 Palaiseau, France

ARTICLE INFO

Article history:
Received 10 May 2010
Accepted 27 July 2010
Available online 3 August 2010

Keywords:
Dip coating
Dynamic meniscus
Lubrication
Wavy film
Wetting

ABSTRACT

As shown by Landau, Levich and Derjaguin, a plate withdrawn out of a wetting bath at low capillary numbers deforms the very top of the liquid reservoir. At this place, a dynamic meniscus forms, whose shape and curvature select the thickness of the film entrained by the plate. In this paper, we measure accurately the thickness of the entrained film by reflectometry, and characterize the dynamic meniscus, which is found to decay exponentially towards the film. We show how this shape is modified when reversing the motion: as a plate penetrates the bath, the dynamic meniscus can "buckle" and present a stationary wavy profile, which we discuss.

1. Introduction

Coating is a widespread industrial process that consists in depositing a liquid film of uniform thickness on a solid [9,13]. It is commonly achieved by extracting a solid from a bath, a process often referred to as dip coating [11,20,22,26]. Dip coating has been extensively studied in various geometries such as tubes, Hele-Shaw cells and fibers [2,14,16] and for various fluid properties [3,19,17,21,8,1,18,15].

Let us describe the different phenomena observed when a vertical plate is moved out of a bath of wetting liquid of density ρ and surface tension γ. At rest, first, a meniscus develops along the plate [5]. Such a static meniscus can be seen in Fig. 1c. Wetting and gravity are responsible for the deformation of the free surface: for a wetting liquid, the contact angle is zero between the solid and the liquid, while gravity imposes a horizontal surface "far" from the wall. Both constraints can be satisfied by curving the interface by a radius R, such that the increase of gravitational energy $\sim\rho g R^4$ is compensated by the decrease of surface energy $\sim\gamma R^2$. This balance indicates that the meniscus size scales as the capillary length a, with $a = \sqrt{\gamma/\rho g}$.

If the solid plate is moved upwards at a velocity $V_0 > 0$, some liquid is entrained as seen in Fig. 1d and e. The first quantitative analysis of this process was done by Landau, Levich and Derjaguin [10,6]. The driving force for entrainment is viscosity: molecules close to the wall follow its motion and entrain their neighbors. The viscous force per unit volume scales as $\eta V_0/h_0^2$, denoting h_0 as the entrained thickness. Two different volumetric forces resist viscous entrainment, namely gravity ρg and surface tension. As emphasized above, the meniscus is curved: according to Laplace, its pressure is lower than the ambient pressure by an amount γ/a. Conversely, the pressure in the entrained flat film (far above the meniscus) is the ambient pressure, which implies a pressure gradient opposing liquid entrainment. The corresponding Laplace force is $\gamma/a\lambda$, where λ is the characteristic length of the dynamic meniscus connecting the static meniscus to the flat film. The ratio between gravity and capillary resistances reduces to λ/a, that is, the ratio between the sizes of the dynamic and static menisci. If $\lambda < a$, capillary resistance dominates gravity. We call it the "capillary wiper" regime since the dynamic meniscus acts as an elastic wiper on a windshield, limiting the film thickness right beyond the wiper (Fig. 1d). In this regime, the balance between viscosity and surface tension leads to: $h_0^2/\lambda \sim aCa_0$, where $Ca_0 = \eta V_0/\gamma$ is the capillary number. Since the static meniscus is hardly deformed by the motion of the wall [4], the curvature of the dynamic meniscus, h_0/λ^2, matches the curvature of the static meniscus $1/a$. This implies a second relation: $\lambda^2 \sim ah_0$. We eventually deduce the film thickness $h_0 \sim aCa_0^{2/3}$ and the length of the dynamic meniscus $\lambda \sim aCa_0^{1/3}$. These expressions are expected to be valid in the small deformation regime $\lambda \ll a$, that is, for $Ca_0 \ll 1$. A rigorous asymptotic matching allowed Landau, Levich and Derjaguin to derive the numerical factors in these laws [10,6]:

$$h_0 \simeq 0.94\ a\ Ca_0^{2/3} \tag{1}$$

$$\lambda \simeq 0.65\ a\ Ca_0^{1/3} \tag{2}$$

* Corresponding author.
E-mail address: clanet@ladhyx.polytechnique.fr (C. Clanet).

0021-9797/$ - see front matter © 2010 Elsevier Inc. All rights reserved.
doi:10.1016/j.jcis.2010.07.069

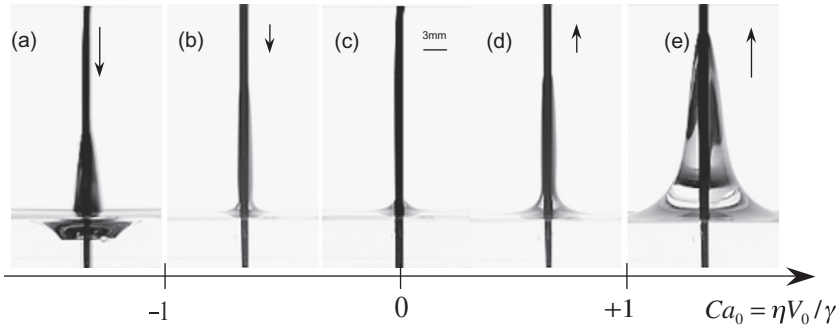

Fig. 1. Deformation of a liquid bath induced by the motion of a vertical solid plate at different capillary numbers $Ca_0 = \eta V_0/\gamma$. $Ca_0 > 0$ corresponds to an upward motion of the plate that comes out coated with a film. Conversely, a plate coated at $Ca_0 > 0$ can be plunged in the bath ($Ca_0 < 0$).

For high capillary numbers, we observe in Fig. 1e that the dynamical meniscus becomes much larger than the static one and that the film has a non-uniform thickness. In this regime, gravity dominates surface tension which leads to the force balance $\eta V_0/h_0^2 \sim \rho g$. As early noticed by Derjaguin, the entrainment law becomes $h_0 \sim aCa_0^{1/2}$. Since the gravitational drainage of a film of thickness h_0 takes place at a velocity $\rho g h_0^2/\eta$, we also deduce that the film falls down at the entrainment velocity V_0, explaining why it cannot reach a uniform thickness.

Once the plate is coated, its motion can be reversed ($Ca_0 < 0$). At small velocity ($-1 < Ca_0 < 0$), the static meniscus is weakly affected by the motion of the wall (Fig. 1b), while it gets inverted at high negative capillary numbers, as seen in Fig. 1a where we observe a centimetre-size black region below the free surface. In this regime, the meniscus shape looks like the one obtained during the impact of liquid jets in a pool of the same liquid [12], and air entrainment may occur [25].

Here, we focus on the domain of small capillary numbers [Fig. 1d and b] and measure the characteristics of the dynamic meniscus for entrainment (Section 2) and immersion (Section 3). For entrainment, we compare the size and shape of the dynamic meniscus to the predictions of Landau–Levich. For immersion, we show how this shape is affected by the direction of the motion, and interpret our results using predictions by Wilson and Jones [25].

2. Dragging a plate out of a wetting liquid

2.1. Measurements of the film thickness

The thickness of the liquid layer was measured by reflectometry. The measurement consists in analyzing the interference fringes of the light reflecting on the different layers of the plate. The various indices of reflection are known, so that the thickness of the liquid layer can be deduced from the analysis of the interference pattern. The spectrum of light wavelength is 400–850 nm. The incident and reflected beams are driven by an optical fiber at a distance of typically 5 mm from the substrate. A spectrometer analyses the light reflected by the substrate: we used silicon wafers, smooth at the atomic scale and reflective like mirrors. The thicknesses accessible by this technique are in the range of 20 nm to 30 μm, with a precision of typically ±3%. Less than 1 second is necessary for acquiring one data point, and the error bars correspond to the data size, in Fig. 2 and others. For films thicker than 10 μm, we complemented the optical technique by weight measurements: the plate was totally extracted from the bath and its mass determined using a precise balance. We checked for three different velocities that the results obtained using the reflectometer and the balance were the same, with a comparable precision.

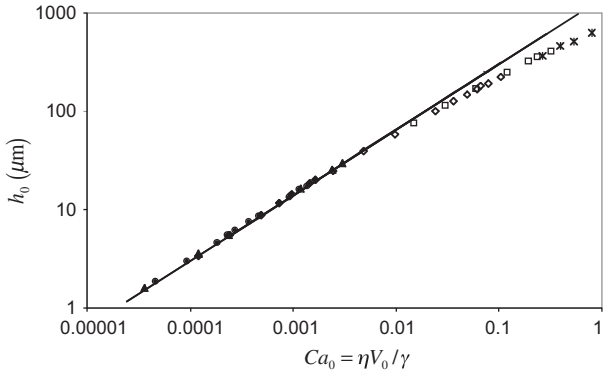

Fig. 2. Thickness h_0 of the film entrained by a silicon wafer extracted at V_0 out of a bath of silicone oil. Full and empty symbols correspond to reflectometry and weight measurements, respectively. The symbols indicate the viscosity of silicone oil (η = 5 mPa s, diamonds; η = 10 mPa s, circles; η = 300 mPa s, squares; η = 1000 mPa s, asterisks), which all have the same surface tension (γ = 20 mN/m), density (ρ = 970 kg/m^3) and capillary length (a = 1.5 mm). The solid line is the Landau–Levich law (Eq. (1)).

As liquids, we used silicone oils (PDMS) of viscosity η from 5 to 1000 mPa s, and constant surface tension γ = 20 mN/m and density ρ = 970 kg/m^3. The corresponding capillary length a is 1.5 mm. Silicone oils totally wet the wafers. The substrates were fixed, and the coating achieved by lowering the reservoir of liquid, using a step-by-step motor and a software to control its displacement. The withdrawal velocities V_0 could be varied between 10 μm/s and 2 cm/s.

We display in Fig. 2 the results of the measurements. The data are compared to the Landau–Levich law (Eq. (1)), and an excellent agreement is found on more than two decades in capillary number ($5.10^{-5} < Ca_0 < 10^{-2}$). The film is always thick enough ($h_0 > 1$ μm) to neglect the role of long range forces, which generally tend to thicken the film in a wetting case. The agreement is not found only for the scaling law ($h_0 \sim Ca_0^{2/3}$), but also for the numerical coefficient.

On the other hand, data for $Ca_0 > 10^{-2}$ deviate from (Eq. (1)) and the deviation increases with Ca_0. For such capillary numbers, the Landau–Levich assumptions are not satisfied anymore and gravity thins the entrained film [24,23,7]. As shown in the introduction, one expects the thickness to scale as $Ca_0^{1/2}$ at high capillary number, in qualitative agreement with the tendency observed at large Ca_0 in Fig. 2. However, a complete theoretical study of this regime remains to be done.

We now discuss the actual shape of the dynamic meniscus, first recalling the classical results of the Landau–Levich analysis and then comparing them to the experimental profiles obtained by reflectometry (see Fig. 3).

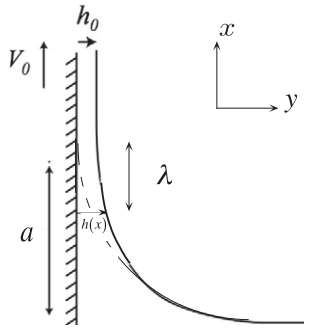

Fig. 3. Sketch of the dynamic meniscus in the withdrawal case. The dotted line shows the position of the static meniscus and λ is the length of the dynamic meniscus connecting the static meniscus to the uniform entrained film.

2.2. The Landau–Levich profile

For small capillary numbers, the Laplace pressure can be simply expressed as $-\gamma d^2h/dx^2$ and the Stokes equation takes the form: $\eta d^2u/dy^2 = -\gamma d^3h/dx^3$, where x and y are the directions along and perpendicular to the velocity u. Integrating this equation with classical boundary conditions [no slip at the solid surface ($y = 0$), negligible viscous stress at the free surface ($y = h$)], a Poiseuille profile is found for the flow: $u(y) = V_0 - \gamma(d^3h/dx^3)y(y - 2h)/(2\eta)$. The film profile being steady, the flux is conserved along x, which can be written:

$$h_0V_0 = hV_0 + \frac{\gamma}{3\eta}\frac{d^3h}{dx^3}h^3 \tag{3}$$

As emphasized in Ref. [10], this equation can be made dimensionless by scaling the film thickness h by h_0, and x by $\lambda = h_0/(3Ca_0)^{1/3}$. Putting $H = h/h_0$ and $X = x/\lambda$, Eq. (3) becomes:

$$\frac{d^3H}{dX^3} = \frac{1-H}{H^3} \tag{4}$$

In order to satisfy the boundary condition $H(X = +\infty) = 1$, we can write close to the film: $H(X) = 1 + \epsilon(X)$ ($\epsilon \ll 1$), which reduces Eq. (4) to: $\epsilon_{XXX} = -\epsilon$. This linear equation admits solutions of the type $\epsilon(X) = \alpha e^{\beta X}$ with $\beta^3 = -1$. The only solution matching the uniform film is $\beta = -1$, which leads to $H = 1 + \alpha e^{-X}$, or:

$$h(x) \simeq h_0\left(1 + \alpha e^{-x/\lambda}\right) \tag{5}$$

In this equation, α is a constant which reflects the invariance of the dynamic meniscus (4) with respect to a translation along X. Eq. (4) can be integrated numerically down to the meniscus region, starting from the asymptotic shape $H = 1 + \alpha e^{-X}$. It is found that H_{XX} saturates at the value 0.644 in the limit $X = -\infty$: at large H, the right hand side of the Eq. (4) quickly vanishes, meaning that d^2H/dX^2 indeed tends towards a constant. This property was exploited by Landau and Levich: matching this constant with the curvature $\sqrt{2}/a$ at the top of the static meniscus allowed them to deduce both the thickness of the entrained film $h_0 \simeq 0.644\sqrt{2}aCa_0^{2/3}$ (Eq. (1)) and the length of the dynamic meniscus $\lambda \simeq 0.644\sqrt{2}/3^{1/3}aCa_0^{1/3}$ (Eq. (2)).

2.3. Measurements of the meniscus characteristics

We measured the stationary shape of the dynamic meniscus during the film deposition by scanning the free surface along the flow with the reflectometer. Fig. 4a shows such a scan, obtained as withdrawing a silicon wafer at $V_0 = 25$ μm/s out of a silicone oil of surface tension $\gamma = 20$ mN/m and viscosity $\eta = 100$ mPa s. The corresponding capillary number is low (1.25×10^{-4}), in the range of applicability of the Landau–Levich laws. We expect from Eq. (1) a thickness $h_0 = 3.5$ μm for the deposited film, in excellent agreement with the value at large x in Fig. 4a. It is also observed that the film is flat, which confirms the negligible role of gravity in the limit of small capillary numbers. In the same figure, the profile is nicely fitted by an exponential function, $h(x) = h_0(1 + \alpha e^{-x/L})$, as expected from Eq. (5). We deduce from the fit a value for L, which for this particular example is found to be 47 ± 1 μm. This value is in good agreement with the length calculated by Eq. (2), which is $\lambda = 47$ μm.

We repeated this experiment for different oil viscosities and withdrawal velocities, which allowed us to vary the capillary number between 10^{-4} and 2×10^{-4}. In each case, the profile of the dynamic meniscus could be nicely fitted by an exponential law, whose characteristic length L is plotted in Fig. 4b as a function of λ, the length calculated from Eq. (2) for each experiment. There again, the fit is quite good (the data scatter around the line $L = \lambda$), without any adjustable parameter. As a conclusion, reflectometry appears to be suitable for quantitatively describing the dynamic meniscus, whose shape directly reflects the hydrodynamics of the problem. Therefore, we can think of using this technique in situations where some added complexity should impact the flow, and

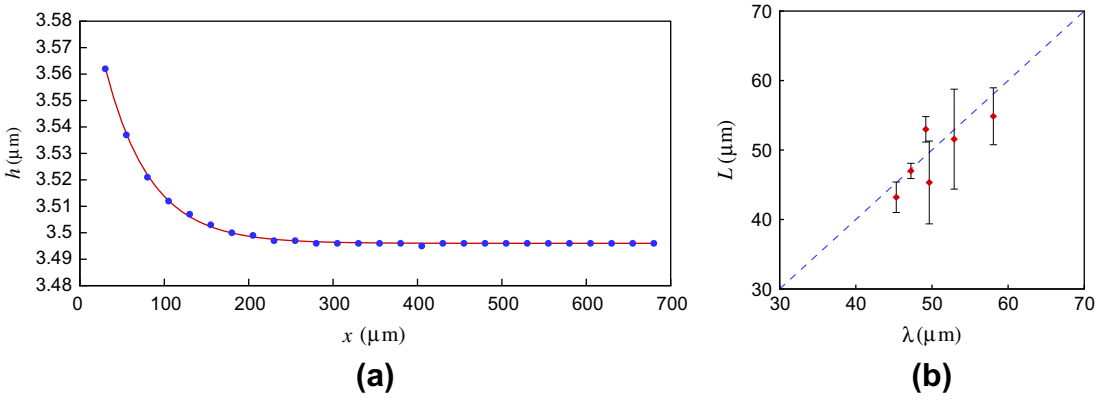

Fig. 4. (a) Stationary profile of the dynamic meniscus in the region of the entrained film obtained by reflectometry, for a silicon wafer drawn at $V_0 = 25$ μm/s out of a bath of silicone oil of surface tension $\gamma = 20$ mN/m and viscosity $\eta = 100$ mPa s. The dots are the data, and the line is an exponential fit of characteristic length $L = 47$ μm. (b) Characteristic length L of the dynamic meniscus deduced from fits such as reported in (a) as a function of the Landau–Levich length λ [Eq. (2)]. The data scatter around the line $L = \lambda$.

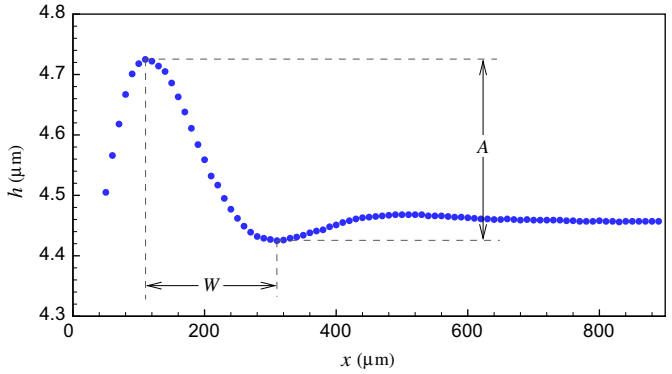

Fig. 5. Stationary profile of the dynamic meniscus, for a plate coated by a thin film ($h_0 = 4.46$ μm) of silicone oil ($\gamma = 20$ mN/m and $\eta = 350$ mPa s) immersed at $V = 10$ μm/s inside a bath of the same silicone oil. The data are obtained by reflectometry. The profile is found to be wavy, with a half-wavelength $W \approx 200$ μm and amplitude $A \approx 0.3$ μm.

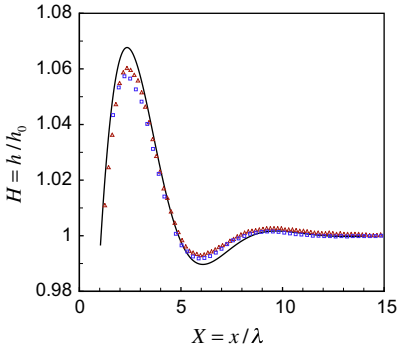

Fig. 6. Stationary profile of the dynamic meniscus, for a plate coated at a velocity V_0 by silicone oil ($\gamma = 20$ mN/m and $\eta = 350$ mPa s) and then immersed at $V = V_0$ inside a bath of the same oil. The film thickness h is scaled by the deposited thickness h_0, and the x coordinate by the length $\lambda = h_0/(3\eta V/\gamma)^{1/3}$ of the dynamic meniscus. The data correspond to $V = 10$ μm/s (triangles) and $V = 20$ μm/s (squares). The line is the numerical solution of Eq. (6), which yields a solution close to Eq. (7), with $\alpha = 1$.

the dynamic meniscus – such as coating with surfactants, with non-Newtonian fluids, or immersion experiments as done below.

3. Driving the wetted plate in the pool

3.1. Observations

We now discuss what happens as immersing at a velocity $-V$ a plate first coated at a velocity V_0 (Fig. 1b). There again, the motion distorts the top of the quasi-static meniscus, but the shape of the interface is found to differ from previously. As shown in Fig. 5, we now observe stationary ripples, instead of the monotonous profile in Fig. 4a: the film (of thickness $h_0 = 4.45$ μm) covering the plate "buckles" in the dynamic meniscus (small values of x). The amplitude A of the wave is a fraction of a micrometer while the wavelength is typically 400 μm. At smaller x, h grows quickly and meets the meniscus, a region not shown in the figure since our reflectometry method only works for small slopes and thin films. We now comment on the origin of such oscillations.

3.2. Wavy Landau–Levich meniscus

At small capillary numbers ($\eta V/\gamma \ll 1$), the only difference with the withdrawing case is a change in sign for the plate velocity. Replacing V_0 by $-V$ in Eq. (4) yields the following equation for the profile [2,25]:

$$\frac{d^3H}{dX^3} = \frac{H-1}{H^3} \tag{6}$$

where h and x are scaled by $h_0 = 0.94a(\eta V_0/\gamma)^{2/3}$ and $\lambda = h_0/(3\eta V/\gamma)^{1/3}$. Close to the film, the linearization of Eq. (6) [$H = 1 + \epsilon X$] leads to $\epsilon_{XXX} = \epsilon$, whose acceptable solutions are $\epsilon(X) = \alpha_1 e^{\beta_1 X}$ and $\epsilon(X) = \alpha_2 e^{\beta_2 X}$ with $\beta_1 = -1/2 + i\sqrt{3}/2$ and $\beta_2 = -1/2 - i\sqrt{3}/2$. The film thickness thus varies as:

$$H(X) = 1 + \alpha e^{-\phi/\sqrt{3}} e^{-X/2} \cos\left(\sqrt{3}X/2 + \phi\right) \tag{7}$$

where the phase ϕ reflects the invariance of the dynamic meniscus (6) with respect to a translation along X. This function indeed shows an oscillatory behavior, damped by an exponential decay as going to the film region. The characteristic length scale for this inverted dynamic meniscus is 2λ. The corresponding wavelength is $4\pi\lambda/\sqrt{3}$, which yields W (defined in Fig. 6) of $2\pi\lambda/\sqrt{3} \simeq 3.6\lambda$. For the particular case of Fig. 5, we have $\lambda = 55$ μm and we measure $W = 200 \pm 5$ μm, in excellent agreement with the expected value of 198 μm.

The linear solution (7) can be used to integrate the non-linear Eq. (6). There again, H_{XX} saturates in the limit $X = -\infty$, at a value depending on α. This is not a surprise because of the independence of the coating and immersion velocities V_0 and V. Using the relation $h_{xx} = h_0/\lambda^2\ H_{XX}$ together with $\lambda = h_0/(3Ca)^{1/3}$, $h_0 = 0.94aCa_0^{2/3}$ and the curvature $\sqrt{2}/a$ at the top of the static meniscus, we get:

$$H_{XX}(-\infty) = 0.64\left(\frac{Ca_0}{Ca}\right)^{2/3} \tag{8}$$

If $Ca = Ca_0$, we recover the former limit $H_{XX} = 0.64$.

3.3. Comparison with the experiments

Eq. (6) suggests to present the results in a dimensionless fashion, which is done in Fig. 6 for two series of data. The data are observed to collapse in a single curve, and this curve is fairly well fitted by the numerical solution of Eq. (6) (solid line), which is solved and matched with the film (this yields a solution very close to Eq. (7) with $\alpha = 1$). The fit nicely captures the period of the wave and slightly overestimates the height of the largest bump. The numerical solution also predicts the existence of a second minimum close to $X = 0$, but, as emphasized earlier, this region could not be characterized experimentally.

In Fig. 6, pre-coating and immersion were performed at the same velocity ($V = V_0$). This situation is the most natural one. It arises in roll coating, where a roller half immersed in a bath drags oil as it turns and re-enters the bath at the same velocity after half a turn. It also corresponds to the case described by Bretherton, where a long bubble is moved in a tube filled with liquid [2]. The front and the rear part of the bubble move at the same velocity: the front region generates a film along the wall, while ripples appear at the rear of the bubble.

We considered other values for the ratio V/V_0, and always observed ripples. We show in Fig. 7 how the ratio V/V_0 controls their amplitude and wavelength. While increasing V/V_0 by a factor 400, the reduced amplitude A/h_0 slowly decreases by a factor 3 while the wavelength increases by a comparable amount. In addition, we calculated the film profile expected from Eq. (7), and deduced the theoretical values of A and W. We report in Fig. 7 the comparison between both these quantities (solid lines) and the measured ones.

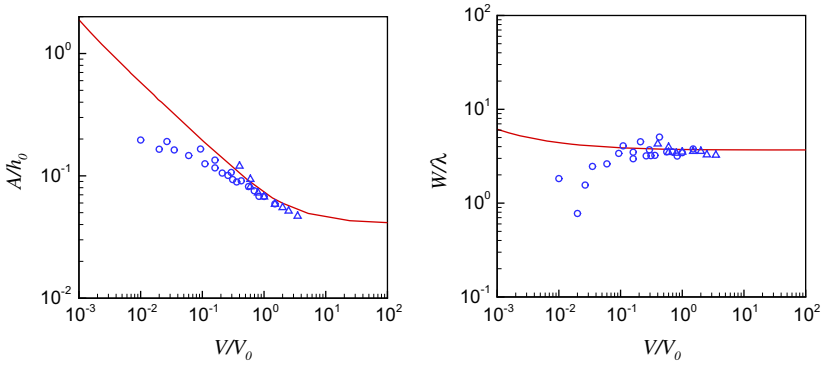

Fig. 7. Amplitude A and half-wavelength W of the wavy meniscus defined in Fig. 5, as a function of the ratio between immersion and withdrawal velocities. A is scaled by h_0 and W by $\lambda = h_0/(3\eta V/\gamma)^{1/3}$, the length of the dynamic meniscus. The oil viscosity η is either 100 mPa s (circles) or 350 mPa s (triangles). The solid lines show the result of the numerical integration of Eq. (6). Deviations are observed at small velocity V, which is interpreted in the text as resulting from gravitational drainage.

The agreement is quite good provided that the ratio V/V_0 is large enough. We see in particular that the dimensionless half-wavelength W/λ tends towards a constant $\simeq$3.5, in excellent agreement with the calculated value $W = 3.6\lambda$. Below $V/V_0 \simeq 0.1$, both the amplitude and the wavelength deviate from the expected values. In this limit, the drainage of the film should perturb the analysis: for $V = 0$ (fixed wall), liquid still enters the pool, yet by a different mechanism (gravitational drainage). Then, as theoretically shown by Wilson and Jones [25], ripples should also exist in the region matching the film and the meniscus.

The transition between Landau–Levich–Bretherton and Wilson–Jones ripples is expected to occur when the drainage velocity V_d of the film exceeds the wall velocity. Since, $V_d \sim \rho g h_0^2/\eta$, this criterion can be written $V/V_0 < (\eta V_0/\gamma)^{1/3}$, independent of g ! For capillary numbers of the order of 10^{-3}, the transition is expected for $V/V_0 < 0.1$, as indeed seen in Fig. 7. In this "fixed wall" limit, gravity can no longer be neglected in the dynamic meniscus and the stationary condition implies:

$$\rho g h_0^3 = \rho g h^3 - \gamma h^3 \frac{d^3 h}{dx^3} \tag{9}$$

Following [25], this equation can be made dimensionless by scaling h by h_0 and x by a new characteristic length $\lambda_g = (a^2 h_0)^{1/3}$. For our micrometric films, we expect λ_g to be in the range of 100–300 μm, as observed experimentally. Eq. (9) then becomes:

$$\frac{d^3 H}{dX^3} = \frac{H^3 - 1}{H^3} \tag{10}$$

Close to the film ($H = 1 + \epsilon$), we obtain $\epsilon_{XXX} = 3\epsilon$, which implies oscillations of half-wavelength $W = 2\pi\lambda_g/3^{5/6}$, i.e. approximately $2.5\lambda_g$, independent of V. This explains why in Fig. 7b the quantity W/λ quickly decreases: W tends towards a constant value, while λ diverges at small V. The study of the evolution of the amplitude A in this small velocity regime remains to be done.

4. Conclusion

We studied by reflectometry the characteristics of Landau–Levich dynamic menisci, that is, the transition region between a static meniscus and a film entrained by a moving solid. If the solid is extracted from the bath, the shape of the "stretched" dynamic meniscus was found to be exponential (close to the film), with a characteristic length slowly increasing as a function of the capillary number (as $Ca_0^{1/3}$), in excellent agreement with the classical Landau–Levich picture. In addition, we could describe in a very wide range of capillary numbers the law of deposition, which provides precise data on plate coating, even at "large" capillary numbers for which gravity also contributes to thin the entrained film.

Once coated, the plate can re-enter the bath. Looking at the common case where the deposition and coating velocities are of the same order, we reported that the dynamic meniscus has a stationary wavy shape. We studied the amplitude, wavelength and envelope of this shape, and found that all these characteristics are quantitatively captured in the Landau–Levich–Bretherton frame. Strong deviations were also observed at small immersion velocities, which were interpreted as resulting from gravitational drainage that also provokes interface undulations, yet of different wavelength as proposed by Wilson and Jones.

Acknowledgments

This work has been supported by The Center for International Research and Collaborations (ISMO).

References

[1] K. Afanasiev, A. Münch, B. Wagner, Phys. Rev. E 76 (2007) 036067.
[2] F.P. Bretherton, J. Fluid Mech. 10 (1961) 166.
[3] B.J. Carroll, J. Lucassen, Chem. Eng. Sci. 28 (1973) 23–30.
[4] X. Chen, E. Rame, S. Garoff, Phys. Fluids 16 (2004) 287–297.
[5] C. Clanet, D. Quéré, J. Fluid Mech. 460 (2002) 131–149.
[6] B. Derjaguin, Comptes Rendus (Doklady) de l'Academie des Sciences de l'URSS 39 (1943) 13–16.
[7] A. de Ryck, D. Quéré, J. Colloid Interface Sci. 203 (1998) 278.
[8] R. Krechetnikov, G.M. Homsy, J. Fluid Mech. 559 (2006) 429–450.
[9] S.F. Kistler, P.M. Schweizer, Liquid Film Coating: Scientific Principles and their Technological Implications, Chapman & Hall, 1997.
[10] L. Landau, B. Levich, Acta Physicochim. URSS 17 (1942) 42–54.
[11] B. Levich, Physical Hydrodynamics, Prentice-Hall, Englewood Cliffs, 1962.
[12] E. Lorenceau, D. Quéré, J. Eggers, Phys. Rev. Lett. 93 (2004) 254501.
[13] F.C. Morey, Natl. Bur. Stand. J. Res. 25 (1940) 385–393.
[14] C.W. Park, G.M. Homsy, J. Fluid Mech. 139 (1984) 291–308.
[15] D. Qu, E. Rame, S. Garoff, Phys. Fluids 14 (2002) 1154–1165.
[16] D. Quéré, Annu. Rev. Fluid Mech. 31 (1999) 347–384.
[17] O.O. Ramdane, D. Quéré, Langmuir 13 (1997) 2911–2916.
[18] E. Ramé, Phys. Fluids 19 (2007) 078102.
[19] J. Ratulowski, H.-C. Chang, J. Fluid Mech. 210 (1990) 303–328.
[20] K.J. Ruschak, Coating flows, Annu. Rev. Fluid Mech. 17 (1985) 65–89.
[21] A.Q. Shen, B. Gleason, G.H. McKinley, H.A. Stone, Phys. Fluids 14 (2002) 4055–4068.
[22] J.H. Snoeijer, J. Ziegler, B. Andreotti, M. Fermigier, J. Eggers, Phys. Rev. Lett. 100 (2008) 244502.
[23] R.P. Spiers, C.V. Subbaraman, W.L. Wilkinson, Chem. Eng. Sci. 29 (1974) 389–396.
[24] D.A. White, J.A. Tallmadge, Chem. Eng. Sci. 20 (1965) 33–37.
[25] S.D.R. Wilson, A.F. Jones, J. Fluid Mech. 128 (1983) 219–230.
[26] S.D.R. Wilson, J. Eng. Math. 16 (1982) 209–221.